ISSN 1392–1207. MECHANIKA. 2016 Volume 22(6): 546–552

A hollow cylindrical linear nut-type ultrasonic motor

Chen Zhuzi*, Chen Yu, Zhou Tieying*****

**Physics Department, Tsinghua University, Beijing, China, E-mail: chenzz11@mail.tsinghua.edu.cn*

***Physics Department, Tsinghua University, Beijing, China, E-mail: chenyu@mail.tsinghua.edu.cn*

****Physics Department, Tsinghua University, Beijing, China, E-mail: zhouty@mail.tsinghua.edu.cn*

crossref http://dx.doi.org/10.5755/j01.mech.22.6.13366

1. Introduction

Ultrasonic motors (USMs) are a new type of motor that uses piezoelectric units to generate ultrasonic vibration in the stator and uses the vibration of the stator to drive the rotor by friction force between the rotor and stator. USMs bear many advantages, such as low speed and large output force, self-locking on power off, quick response, high positioning precision, and excellent electromagnetic compatibility.

According to the motion type, USM can be classified into linear ultrasonic motors (LUSM) and rotary ultrasonic motors. LUSM have rapidly developed in recent years. They are widely applied in areas such as semiconductor manufacturing, aeronautic and astronautic appliances, precise position stages, biomedical equipment, optic fiber alignment facilities, and miniaturized information systems [1].

LUSMs utilizing bending modes of a beam were proposed under direct inspiration of the idea of the disk type travelling wave rotary USM. Both travelling wave and standing wave excitation methods have been developed for this type of motor [2-4]. An LUSM utilizing the L1-B2 mode of a plate has attracted attention for its explicit working mechanism [5-8]. Elliptical motions are formed on one or two tips on the stator to drive the slider. The LUSMs operating in L1-B2 mode have been commercialized by Nanomotion Company and are being applied to many engineering cases and as precise actuators. The V-type or U-type motors have also been the focus of extensive research due to the simple structure. These motors utilize the symmetric and asymmetric mode of two piezoelectric transducers as working modes. The two transducers form an angle or a parallel hinge. When the two transducers are excited with a 90-degree temporal phase difference, an elliptic motion is generated at the tip of the angle or hinge [9-13]. These three motor types are complicated because of the separate slider and stator. Thread-drive LUSM is a comparatively new LUSM, which uses the wobbling motion or in-plane modes of a tube through thread contact. The mover is contained in the stator, making its structure compact. New Scale developed a thread-drive, tube-type LUSM named SQUIGGLE, which utilizes two degenerate, first-order bending modes of a slim tube [14-15]. A two-degrees of freedom fiber optic positioning mechanism, named Cobra, has been developed based on the SQUIGGLE motor [16]. The Cobra mechanism will be mounted on the Subaru telescope on Mauna Kea, Hawaii for positioning optical fibers to allow observations of cosmologic targets.

Many demands for hollow mini motors have emerged in wide areas, such as precise optical instruments, modern medical devices, and precise machining devices, where a hole is needed for light transmission, optic cable [17], or electric wire. We have developed a thread-drive, nut-type travelling wave LUSM that utilizes the two second-order or third-order bending modes in the section plane [18-20]. The stator and rotor are both hollow. The motor is easy to minimize. It is appropriate for autofocusing and zooming in cell phone cameras, microsurgery manipulation, MRI, and mechanical tuning for high temperature superconductor filters and precision instruments. In this paper, stators with four PZT plates and with eight PZT plates are studied. For the stator with four PZT plates, the number of PZT plates used is reduced to increase the vibration amplitude and improve the motor performance because the PZT has larger internal loss than brass, and extra PZT plates add to the stiffness of the stator. The internal loss and stiffness are both impeding aspects for the resonant vibration amplitude of the stator.

2. Working principle and design of the stator

2.1. Working mechanism

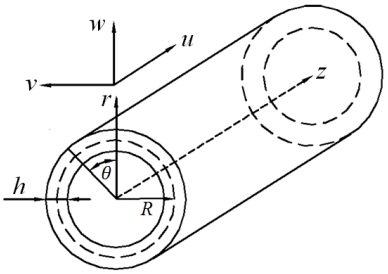

Fig. 1 The theoretical model of the nut-type stator

The nut-type ultrasonic motor utilizes two degenerate bending modes in the section plane of a cylindrical shell to generate a travelling wave transmitting along the circumference. The plane strain vibration equations of a cylindrical shell in a cylindrical coordinate system with coordinates $r-\theta-z$ are: [1]

$$-\frac{R^2\left(1-\mu^2\right)}{E}\rho h\frac{\partial^2 v}{\partial t^2}+\frac{\partial^2 v}{\partial\theta^2}+\frac{\partial w}{\partial\theta}+ +k\left(\frac{\partial^2 v}{\partial\theta^2}-\frac{\partial^3 w}{\partial\theta^3}\right)=0\ ; \tag{1a}$$

$$\frac{R^2\left(1-\mu^2\right)}{E}\rho h\frac{\partial^2 w}{\partial t^2}+\frac{\partial v}{\partial\theta}+w-k\left(\frac{\partial^3 v}{\partial\theta^3}-\frac{\partial^4 w}{\partial\theta^4}\right)=0\ , \tag{1b}$$

where v and w are the circumferential and radial displacement, denotes the thickness of the shell, ρ denotes the mass density, and R is the radius of the neutral surface (Fig. 1). μ is Poisson's ratio, E is Young's modulus, and $k = h^2/12R^2$.

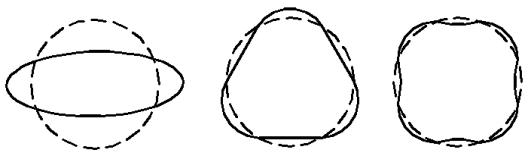

a b c

Fig. 2 The mode shapes in a section plane for a - $n = 2$; b - $n = 3$; c - $n = 4$

The equations have the following solutions:

$$\begin{pmatrix} v_{n1} \\ w_{n1} \end{pmatrix} = A_{n1} \begin{pmatrix} \sin n\theta \\ B_n \cos n\theta \end{pmatrix} \cos \omega t ; \tag{2a}$$

$$\begin{pmatrix} v_{n2} \\ w_{n2} \end{pmatrix} = A_{n2} \begin{pmatrix} \cos n\theta \\ -B_n \sin n\theta \end{pmatrix} \cos \omega t , \tag{2b}$$

where ω is the angular frequency, and A_{n1}, A_{n2} and B_n correspond to the amplitudes. The two solutions correspond to two degenerate nth order radial bending vibration modes in section plane ($r - \theta$ plane). The initial three modes are given for $n = 2$, 3, 4, and they are shown in Fig. 2.

By substituting the solutions into the vibration equation, the following frequency equations can be obtained.

$$\begin{vmatrix} \frac{K}{\rho h R^2}(1+k)n^2 - \omega_n^2 & \frac{K}{\rho h R^2} n\left(1+kn^2\right) \\ \frac{K}{\rho h R^2} n\left(1+kn^2\right) & \frac{K}{\rho h R^2}\left(1+kn^4\right) - \omega_n^2 \end{vmatrix} = 0 . \tag{3}$$

The solution of the above equation is the resonant frequencies of the modes, that is:

$$\omega_n^2 = \frac{1}{2}\frac{K}{\rho h R^2}\left[(1+k)n^2 + kn^4 - \sqrt{\left[(1+k)n^2 + kn^4\right]^2 + 4n^2\left(1+kn^2\right)^2 - 4n^2(1+k)\left(1+kn^4\right)}\right]. \tag{4}$$

The working modes used here are the two degenerate 3rd bending modes in the section plane (Fig. 3).

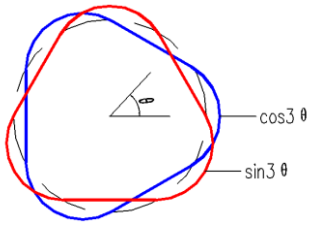

Fig. 3 The 3rd-order bending modes in the $r - \theta$ plane

When the two working modes are excited equally with phase difference $\pi/2$ in time, a travelling wave is generated in the stator. The displacement of a cylindrical shell with travelling wave can be expressed as:

$$\begin{pmatrix} v \\ w \end{pmatrix} = A \begin{pmatrix} \cos(\omega t - 3\theta) \\ B_3 \sin(\omega t - 3\theta) \end{pmatrix}. \tag{5}$$

Thus, the relationship between the displacements in the r and θ directions can be determined as:

$$\frac{v^2}{1} + \frac{w^2}{B_3^2} = A^2 , \tag{6}$$

where A is the amplitude of the travelling wave in the stator. The above equation indicates that the trajectories of points on the inner surface of the stator are elliptical. Eq. (5) shows that the trajectories are of the same clock direction. When a cylindrical rotor is placed inside the stator and their surfaces form a cylindrical contact pair, the travelling wave in the stator drives the rotor to rotate.

2.2. The mechanical quality factor Q of the stator

The stator of a USM is actually a piezoelectric transducer. The mechanical quality factor Q is an important factor to evaluate a piezoelectric transducer. Q is the ratio of the mechanical energy stored in the stator to the mechanical energy loss in the stator in a vibration period, as Eq. 7 shows:

$$Q = 2\pi \frac{W_m}{\Delta W_m} . \tag{7}$$

Thus, the Q factor is positively correlated with the energy efficiency of the stator. For the same stator structure and load, a higher Q factor indicates a higher energy efficiency. Furthermore, the magnitude of Q is very important in evaluating the magnitude of the resonant strain. The vibration amplitude at an off-resonance frequency is amplified by a factor proportional to Q at the resonance frequency. It can be calculated from the impedance spectrum according to the following equations:

$$Q = \frac{f_r}{f_1 - f_2} . \tag{8}$$

In which, f_r is the resonant frequency of the stator, and f_1 and f_2 are the upper and lower half-power frequencies.

2.3. Design of the hollow nut-type motor

The hollow, linear, nut-type ultrasonic motor consists of three parts: a metallic main body, a rotor and piezoelectric elements as shown in Fig. 4. The elastic body is a nut-type, metal tube, which has threads on the inside surface and eight flat surfaces on the outside surface. The rotor is a hollow threaded screw, whose threads match that of the stator, so that only relative helical motion is allowed between the stator and the rotor. The piezoelectric elements are rectangular sheets polarized in the thickness direction. They are bonded to the external faces of the octagon metal tube to form a stator. Because the wall of the stator is very thin and the thickness to radius ratio is very small, a theoretical

model of the stator can be simplified as a cylindrical shell, as analyzed in Section 2.1 (Fig. 2). The stator utilizes two 3rd-order bending modes in the section plane as working modes to form a travelling wave. The thread contact pair between the rotor and stator then transforms the rotation of the rotor into helical motion (linear and synchronous rotation).

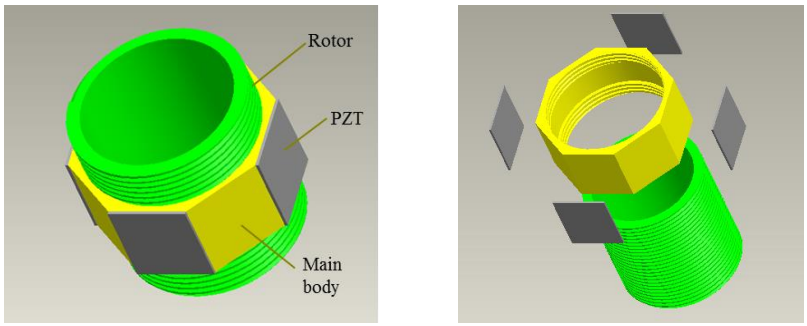

a b

Fig. 4 Structure of the hollow, linear, nut-type ultrasonic motor: a - assembly view; b - exploded view

Table 1

Physical and electrical properties of PZT

Stator	Young's modulus, GPa	Young's modulus along 33, GPa	Young's modulus along 11, GPa	Young's modulus along 55, GPa	Poisson's ratio	Density, kg m^{-3}	Piezoelectric constant, d_{31}, $\times 10^{-12}$ mV^{-1}	Quality factor	Loss coefficient
Brass	1.15	–	–	–	0.3	8900	–	–	0.002
PZT5	–	0.63	0.76	0.23	–	7500	−274	60	0.0166

A stator with four PZT plates and a stator with eight PZT plates were fabricated. The stator with four PZT plates was proposed for consideration of the increased vibration amplitude and improved motor performance. Because PZT ceramics have considerably larger mechanical loss than brass, as observed from Table 1, four PZT plates may output larger net output power, even though the total input electrical energy is smaller for a reduced conversion capability.

3. Experiments

Prototype nut-type motors with four and eight PZT plates were fabricated. Octagon nut-type ultrasonic stators with 12 mm thread diameter, 0.5 mm thread pitch, 5 mm side length, and 6-mm height were fabricated (Fig. 5). The thickness of the PZT plates was 0.2 mm. The electromechanical converting elements were PZT5 ($Pb(Ti_xZr_{1-x})O_3$). They were bonded to the stator body with epoxy gel. The stator body was made of brass and acts as the common electrical ground for all PZT plates. The characteristics of the materials used are listed in Table 1. The table shows that the PZT5 has a larger loss coefficient than that of brass. PZT plates were polarized and connected, as shown in Fig. 6. The group of PZT plates connected to the *cos ωt* signal excites the 3rd-order bending modes in the section plane, and the group of PZT plates connected to the *sin ωt* signal excites the other working mode, with a $\pi / 2$ phase difference in the time domain.

Taking each PZT plate as a standing wave source, the travelling wave generated in the stator with four PZT plates can be calculated as:

$$u_r = A\left[\sin 3\theta \sin \omega t + \sin\left(3\theta - \frac{3\pi}{2}\right)\cos \omega t - \right.$$
$$\left. - \sin(3\theta - 3\pi)\sin \omega t - \sin\left(3\theta - \frac{9\pi}{2}\right)\cos \omega t\right] =$$
$$= 2A\cos(\omega t - 3\theta), \quad (9)$$

where u_r is the displacement in the radial direction. The travelling wave generated in the stator with eight PZT plates can be calculated as:

$$u = A\left[\sin 3\theta \sin \omega t - \sin\left(3\theta - \frac{3\pi}{4}\right)\sin \omega t + \sin\left(3\theta - \frac{6\pi}{4}\right)\cos \omega t - \sin\left(3\theta - \frac{9\pi}{4}\right)\cos \omega t - \sin\left(3\theta - \frac{12\pi}{4}\right)\sin \omega t + \right.$$
$$\left. + \sin\left(3\theta - \frac{15\pi}{4}\right)\sin \omega t - \sin\left(3\theta - \frac{18\pi}{4}\right)\cos \omega t + \sin\left(3\theta - \frac{21\pi}{4}\right)\cos \omega t\right] = 3.7A\sin\left(\omega t - 3\theta - \frac{3\pi}{8}\right). \quad (10)$$

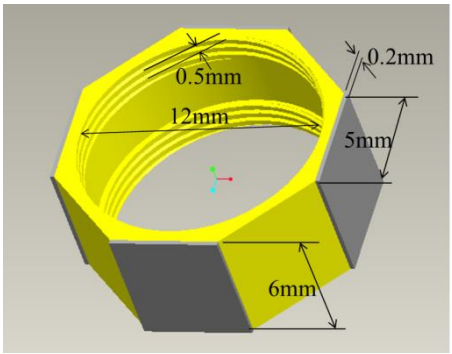

Fig. 5 Dimensions of the stator

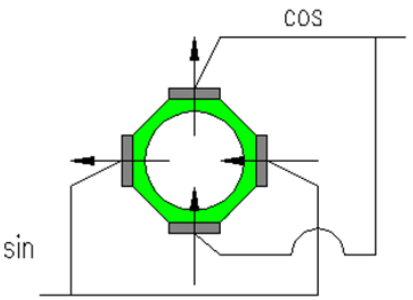

a

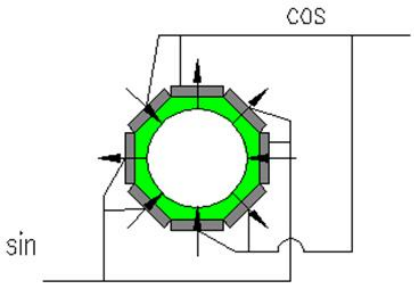

b

Fig. 6 The practical polarizing and connection of the stators: a - polarizing and connection of the stator with four PZT plates; b - polarizing and connection of the stator with eight PZT plates

3.1. Modal analysis and impedance spectrum measurement

Table 2

Parameters obtained from the impedance spectrum measurement

Numberof PZT	f_r, Hz	f_1, Hz	f_2, Hz	Q
Four	16400	16364	16443	208
Eight	18184	18114	18262	128

Modal analysis of the two stators was conducted using commercial finite element method software (Figs. 7-8). All studied structures showed the same 3rd-order bending modes in the $r - \theta$ plane. The resonant frequencies of the stators are 16345 Hz and 18359 Hz for the structures with four and eight PZT plates, respectively. The results are close to the resonant frequencies obtained from the impedance spectrum measurement.

The electrical impedance spectra of the stators were measured with an electrical dynamic impedance analyzer (4294A. Agilent Inc.). The mechanical quality factor was calculated automatically by the software on the PC according to Eq. 8. The results are listed in Table 2. From Table 2, the stator with four PZT plates has a higher Q factor, which is favorable for the vibration amplitude and energy efficiency. The stator with four PZT plates will be more efficient than the stator with eight PZT plates.

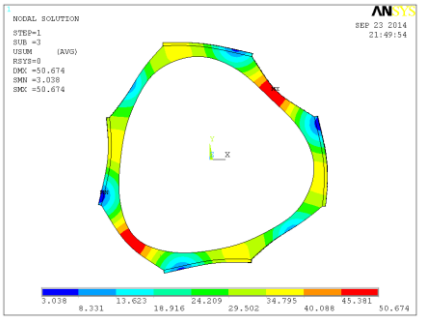

a

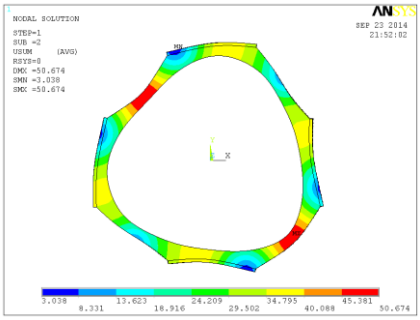

b

Fig. 7 The simulated 3rd-order bending modes in the section plane of the stator with four PZT plates: a - mode A; b - mode B

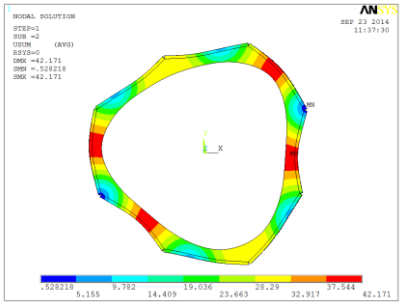

a

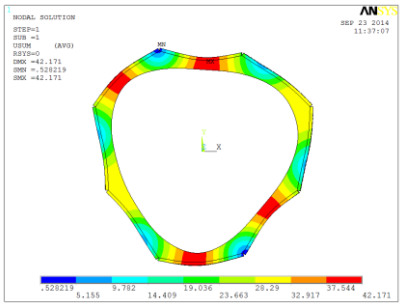

b

Fig. 8 The simulated 3rd-order bending modes in the section plane of the stator with 8 PZT plates: a - mode A; b - mode B

3.2. Amplitude and energy consumption rate of the stators

The stator vibration amplitude was measured with a laser vibrometer (Polytec OFV50X) at a free boundary condition without the rotor at different frequencies under 0.1 V peak-peak excitation (Fig. 9). The radial displacements of points on the side plate of the stator were measured around their resonant frequencies with electrodes connected as shown in Fig. 6. The measured points are the antinodes with the largest amplitude. Only one of the two groups shown in Fig. 6 was connected to excite a single mode.

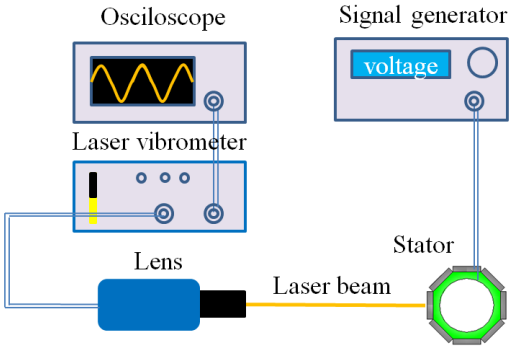

Fig. 9 The schematic diagram of measuring stator amplitude

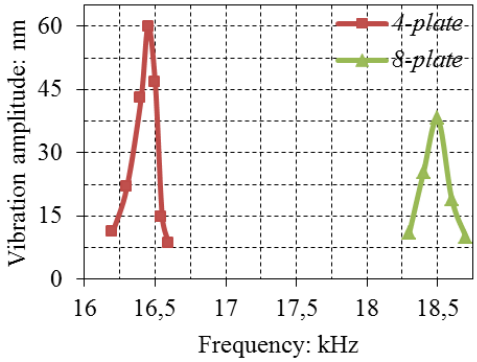

Fig. 10 Measured frequency response of the assembled stators

Fig. 10 shows that the vibration amplitude of the stator with four PZT plates at resonance is significantly increased. The results are consistent with the Q factor measurement in Table 2. Keeping some areas without bonded PZT plates helps to enlarge the vibration amplitude.

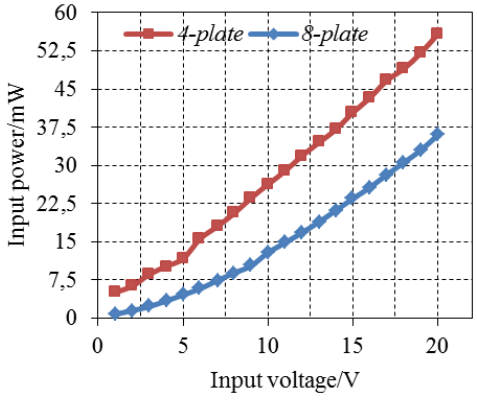

Fig. 11 The input power of the stators in the free condition

The electrical input power of the free stator was tested with an oscilloscope by multiplying the current and voltage and averaging their product. The input power of each group of PZT plates of a motor was tested independently, and the total input power was obtained by adding both groups.

The results show that the stator with eight PZT plates consumes more electrical power (Fig. 11), indicating that it has a larger internal energy loss, and the stator with four PZT plates is more efficient when the same load is applied, which is in agreement with the Q factor measured in Section 3.1.

3.3. Performance of the hollow, linear, nut-type, ultrasonic motors

A dual channel signal generator was employed to drive the motor. A 10 V peak-peak, AC excitation with 90 degree time phase difference was applied to the motor. The moving speed of the rotor was measured with a photoelectric velocity detector and an encoding disk with 100 lines that was attached to the rotor (Fig. 12). When the rotor rotates, the code disk triggers the photoelectric velocity detectors to generate square waves. The frequency of the square wave is proportional to the rotation speed, and the speed can be read out from an oscilloscope. The thread pitch of the stator and rotor is 0.5 mm; thus, the linear moving speed can be calculated by multiplying the rotation speed by 0.5 mm/round.

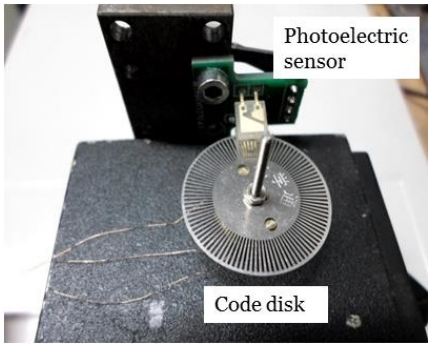

Fig. 12 Setup for measuring the moving speed

To characterize the load characteristics of the motor, the moving speed of the motor was measured with rotors of different weights because the rotor weight also acts as a pre-press for the friction between the rotor and stator. A 10 V peak-peak and AC driving voltages of 16.4 kHz and 18.2 kHz were applied to the two motors according to the resonant frequencies obtained from the modal and impedance spectrum analysis in Section 3.1. The results are shown in Fig. 13.

The motor with four PZT plates moves faster when the rotor weight is below 20 g, whereas the motor with eight PZT plates moves faster when the rotor weighs more than 20 g, which is 16.7 times the weight of the stator, covering most applications for such a stator of 12-mm outer diameter and 1.2 g weight. The stator with four PZT plates is more sensitive to pre-press, which can be comprehended in terms of the Q factor shown in Table 2. The Q factor of the stator with four PZT plates is higher, which plays a dominant role under lower load force. The stator with eight PZT plates has a larger volume of driving units, providing larger driving capacity. The driving capacity plays a dominant role under heavy load force. The motor with four PZT plates obtained

an upward speed of 0.95 mm/s when the load force was 3 g, and the maximum thrust force was 0.35 N. The weight of the stator was 1.2 g, and the maximum thrust force to weight ratio was 29.1:1. The downward and upward performances show a difference in their operating speed. Due to gravity, the downward operating speed is higher than the upward speed.

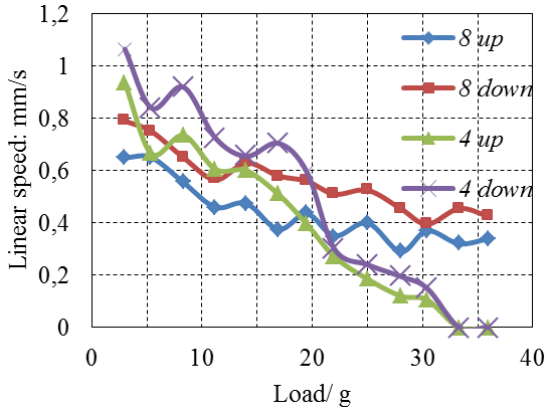

Fig. 13 Performance of the hollow, linear, nut-type, ultrasonic motors

4. Conclusion

A hollow, nut-type, linear USM has been reported in this paper. The motor uses two 3rd-order bending modes in a section plane as working modes. Two stators with different numbers of PZT plates were studied. The working modes of the two stators were analyzed theoretically and were observed with finite element method software. Two prototype stators with four and eight PZT plates were fabricated and tested with an impedance analyzer. The stator with four PZT plates is simpler than the stator with eight PZT plates and has a higher mechanical quality factor, vibrates at a larger amplitude and is more energy efficient. The motor showed better performance than the eight plate stator when working under loads of 20 g, which covers most application conditions for a stator with a 12-mm outer diameter. At 10 V peak-peak excitation, the motor with four PZT plates obtained an upward speed of 0.95 mm/s when the load force was 3 g, and the maximum thrust force was 0.35 N. The maximum thrust force to weight ratio was 29.1:1.

The stator and rotor of the motor are both cylindrical and hollow, making it appropriate for applications where a light path, electric wire or optic fiber needs to pass through the motor. Other working parts can be contained in the hollow space inside the rotor and stator.

Acknowledgements

This work was supported by the National Natural Science Foundation of China (No. 51077086; 11334005).

References

1. **Zhao, C.** 2011. Ultrasonic Motors, Springer Berlin Heidelberg,494 p. http://dx.doi.org/10.1007/978-3-642-15305-1.
2. **Siyuan, H.; Weishan, C.; Xie, T.** 1998. Standing wave bi-directional linearly moving ultrasonic motor, IEEE Transactions on Ultrasonics, Ferroelectrics, and Frequency Control 45(5): 1133-1139. http://dx.doi.org/ 10.1109/58.726435.
3. **Vyshnevsky, O.; Kovalev, S.; Wischnewskiy, W.** 2005. A novel, single-mode piezoceramic plate actuator for ultrasonic linear motors, IEEE Transactions on Ultrasonics, Ferroelectrics, and Frequency Control 52(11): 2047-2053. http://dx.doi.org/10.1109/TUFFC.2005.1561674.
4. **Roh, Y.; Lee, S.; Han, W.** 2001. Design and fabrication of a new traveling wave-type ultrasonic linear motor, Sensors & Actuators: A. Physical 94(3): 205-210. http://dx.doi.org/10.1016/j.sna.2004.01.019.
5. **Ming, Y.; Meiling, Z.; Richardson, R.C.** 2005. Design and evaluation of linear ultrasonic motors for a cardiac compression assist device, Sensors and Actuators A: Physical 119(1): 214-220. http://dx.doi.org/10.1016/j.sna.2004.09.005.
6. **Shi, S.; Chen, W.; Liu, J.** 2006. A high speed ultrasonic linear motor using longitudinal and bending multimode bolt-clamped Langevin type transducer, 2006 International Conference on Mechatronics and Automation, 612-617. http://dx.doi.org/10.1109/ICMA.2006.257641.
7. **Ming, Y.; Hanson, B.; Levesley, M.** 2006. Amplitude modulation drive to rectangular-plate linear ultrasonic motors with vibrators dimensions 8 mm /spl times/ 2.16 mm /spl times/ 1 mm, IEEE Transactions on Ultrasonics, Ferroelectrics and Frequency Control 53(12): 2435-2441. http://dx.doi.org/10.1109/TUFFC.2006.191.
8. **Shi, Y.; Zhao, C.** 2011. A new standing-wave-type linear ultrasonic motor based on in-plane modes, Ultrasonics 51(4): 397-404. http://dx.doi.org/10.1016/j.ultras.2010.11.006.
9. **Hemsel, T.; Mracek, M.; Wallaschek, J.** 2004. A novel approach for high power ultrasonic linear motors, IEEE Ultrasonics Symposium 2: 1161-1164. http://dx.doi.org/10.1109/ULTSYM.2004.1417988.
10. **Borodin, S.; Kim, J.; Kim, H.** 2004. Nano-positioning system using linear ultrasonic motor with “shaking beam”, Journal of Electroceramics 12(3): 169-173. http://dx.doi.org/10.1023/B:JECR.0000037722.27973.d3.
11. **Fan, Z.; Weishan, C.; Junkao, L.** 2005. Bidirectional linear ultrasonic motor using longitudinal vibrating transducers, IEEE Transactions on Ultrasonics, Ferroelectrics, and Frequency Control 52(1): 134-138. http://dx.doi.org/10.1109/TUFFC.2005.1397358.
12. **Fernandez, J.M.; Perriard, Y.** 2006. Sensitivity analysis and optimization of a standing wave ultrasonic linear motor, IEEE Transactions on Ultrasonics, Ferroelectrics and Frequency Control 53(7): 1352-1361. http://dx.doi.org/10.1109/TUFFC.2006.1665084.
13. **Jeong, S.S; Chong, H.H.; Lim, J.H.** 2013. Design of a nib-shaped ultrasonic motor for auto-focusing camera, Integrated Ferroelectrics 141(1):50-57. http://dx.doi.org/10.1080/10584587.2013.778736.
14. **David Henderson, James Guelzow, Conrad Hoffman, Robert Culhane**. Mechanism comprised of ultrasonic lead screw motor. US 11/262,137, US Patent, US20060049720 A1., 2006 03 09.
15. **Henderson, D.A.** 2006. Simple ceramic motor inspiring smaller products, In: Actuator 2006: 10th International

Conference on New Actuators, Bremen, 1-4 p. http://www.newscaletech.com/doc_downloads/Henderson-Actuators%202006.pdf.
16. **Fisher, C.; Braun, D.; Kaluzny, J.** 2009. Cobra: a two-degree of freedom fiber optic positioning mechanism, IEEE Aerospace Conference, 1-11p. http://dx.doi.org/10.1109/AERO.2009.4839435.
17. **Chen, T.; Zhang, N.; Huo, T.** 2013. Tiny endoscopic optical coherence tomography probe driven by a miniaturized hollow ultrasonic motor, J Biomed Opt. 18(8): 86011-1-86011-5. http://dx.doi.org/10.1117/1.JBO.18.8.086011.
18. **Zhou, T.; Chen, Y.; Lu, C.** 2009. Integrated lens autofocus system driven by a nut-type ultrosonic motor (USM), Science in China Series E: Technological Sciences 52(9): 2591-2596. http://dx.doi.org/10.1007/s11431-009-0246-6.
19. **Chen, Z.; Chen, Y.; Zhou, T.** 2015. A nut-type ultrasonic motor driven with single phase signal, Vibration Engineering and Technology of Machinery, 23: 835-843. http://dx.doi.org/10.1007/978-3-319-09918-7_74.
20. **Zhou, T.; Zhang, Y.; Chen, Y.** 2009. A nut-type ultrasonic motor and its application in the focus system, Chinese Science Bulletin 54(20): 3778-3783. http://dx.doi.org/10.1007/s11434-009-0593-5.

Chen Zhuzi, Chen Yu, Zhou Tieying

A HOLLOW CYLINDRICAL LINEAR NUT-TYPE ULTRASONIC MOTOR

A hollow, linear, nut-type, ultrasonic motor based on two degenerate, 3rd-order bending modes in the section plane of cylinders is presented in this paper. The stator and rotor of the motor are both cylindrical and hollow, making the motor appropriate for applications where a light path, electric wire or optic fiber is required to pass through the motor. A new structure with four PZT plates bonded on the stator is proposed here. and the other had all eight sides bonded with PZT plates. The results show that the new design with four PZT plates has a higher mechanical quality factor, vibrates with larger amplitude, and has comparable performance to the stator with eight PZT plates. The motor with four PZT plates reached an upward speed of 0.95 mm/s when the load force was 3 g, and the maximum thrust force was 0.35 N.

Two stators were fabricated and studied.

Keywords: Hollow, linear, nut-type, ultrasonic motor; energy efficiency; mechanical quality factor.

Received November 06, 2015
Accepted November 25, 2016